# Collisional transport and poloidal asymmetry distribution of impurities in tokamak plasmas, with application to WEST

P. MAGET[1], P. MANAS[1], R. DUMONT[1], J-F. ARTAUD[1], C. BOURDELLE[1], L. COLAS[1], M. GONICHE[1], X. GARBET[1], and the WEST Team ♯
[1] CEA, IRFM, F-13108 Saint Paul-lez-Durance, France.
♯ http://west.cea.fr/WESTteam
e-mail contact of main author: patrick.maget@cea.fr

J. FRANK[2,1], O. AGULLO[2]
[2] Aix-Marseille Université, CNRS, PIIM UMR 7345, F-13397 Marseille Cedex 20, France.

T. NICOLAS[3], H. LÜTJENS[3]
[3] Centre de Physique Théorique, Ecole Polytechnique, Institut Polytechnique de Paris, Route de Saclay, 91128 Palaiseau, France.

**Abstract** We report in this contribution on the development of an analytic model for a self-consistent determination of the poloidal asymmetry, collisional flux and steady state profile of heavy impurities [1]. The model is compared with nonlinear axisymmetric simulations with the XTOR code [2, 3, 4], and with computations using the drift-kinetic code NEO [5]. An application to Tungsten peaking in the WEST tokamak under Ion Cyclotron Resonance Heating (ICRH) exemplifies the complex balance between accumulation and expulsion forces at play.

## 1 COLLISIONAL IMPURITY TRANSPORT

The use of metallic walls as plasma facing components in tokamaks puts severe constraints on the control of impurity contamination. Heavy impurities like Tungsten are of particular concern due to the high level of radiative losses they can induce. Moreover, their high sensitivity to neoclassical transport mechanisms exacerbated by toroidal rotation or electrostatic potential asymmetry generally explains experimental cases of strong accumulation in the plasma core. The poloidal distribution of the impurity modulates the amplitude of this neoclassical transport [6], with an asymmetry that often leads to enhancement, but that can also result in a reduction of the flux [7]. Three main mechanisms drive the poloidal asymmetry of the impurity: centrifugal forces, electrostatic potential asymmetry and collisional friction with the main ion. A geometrical formulation of this problem can be derived that relates the horizontal and vertical asymmetry parameters of the impurity density ($n_a$) with the ion density and temperature gradients, toroidal rotation, electrostatic potential asymmetry and collisions [1]. This allows deriving a self-consistent analytical model, implemented in the FACIT code (for FAst Collisional Impurity Transport) that allows a fast computation compatible with integrated modeling needs. We will first describe briefly this model.

The neoclassical flux of an impurity species "a" in the Pfirsh-Schlüter regime can be approximated as

$$\begin{aligned}\langle \Gamma_a^{neo} \cdot \nabla r \rangle \;\approx\; & -\langle n_a \rangle \, \frac{D_{PS}^a}{R_0} \left[ \left( 1 + \frac{\delta}{\epsilon} + \frac{\delta^2 + \Delta^2}{4\epsilon^2} \right) \mathcal{G} + \frac{1}{2} \left( \frac{\delta}{\epsilon} + \frac{\delta^2 + \Delta^2}{2\epsilon^2} \right) \mathcal{U} \right. \\ & \left. - \frac{\delta_M}{2\epsilon^2} \left( 1 - \frac{m_i}{m_a} \frac{e_a}{e_i} \right) \left( 1 + \frac{\delta}{2\epsilon} \right) \right] \end{aligned} \tag{1}$$

with $D_{PS}^a \equiv 2q^2 m_a \nu_a T_a / (e_a^2 \langle B^2 \rangle)$, an asymmetry of the impurity noted as $n_a / \langle n_a \rangle = 1 + \delta \cos\theta + \Delta \sin\theta$, with $\theta$ the poloidal angle, $\epsilon = r/R_0$ and $R_0$ the major radius of the magnetic axis, $\delta_M = 2\epsilon (m_a/m_i)(T_i/T_a) M_i^2$ with $M_i$ the ion Mach number, and

$$\mathcal{G} \;\equiv\; R_0 \left[ \partial_r \ln p_a - \frac{T_i}{T_a} \frac{e_a}{e_i} \partial_r \ln p_i + C_0^a \frac{T_i}{T_a} \frac{e_a}{e_i} \partial_r \ln T_i \right] \tag{2}$$

$$\mathcal{U} \;\equiv\; -R_0 \left( C_0^a + k_i \right) \frac{e_a}{e_i} \partial_r \ln T_i \tag{3}$$

with $C_0^a \approx 1.5$ for heavy impurities and $k_i$ a scalar depending on the ion collisional regime ($k_i \approx -1.17$ in the banana regime). The poloidal asymmetry of the impurity is given by the parallel force balance equation:

$$\delta + \delta_\phi^a - \delta_M \;=\; -\mathcal{A} \left[ \Delta \mathcal{G} + \Delta \mathcal{U} - \mathcal{R} \delta_M \epsilon \Delta \right] \tag{4}$$

$$\Delta + \Delta_\phi^a \;=\; \mathcal{A} \left[ (2\epsilon + \delta) \, \mathcal{G} + \delta \mathcal{U} - 2\mathcal{R} \delta_M \right] \tag{5}$$

with $\mathcal{A} = q^2 \nu_a / (\epsilon \Omega_a)$ with $\Omega_a = e_a B / m_a$, $\mathcal{R} = \frac{1}{2\epsilon} \left( 1 - \frac{m_i}{m_a} \frac{e_a}{e_i} \right)$ and

$$\left( \delta_\phi^a, \; \Delta_\phi^a \right) = Z_a (T_e/T_a) \left( \delta_\phi, \; \Delta_\phi \right)$$

where the electrostatic potential asymmetry is described as $e(\phi - \langle \phi \rangle)/T_e = \delta_\phi \cos\theta + \Delta_\phi \sin\theta$. The parameter $\mathcal{A}$ measures the collisional friction, $\mathcal{G}$ the radial gradients, $\mathcal{U}$ the ion temperature gradient, and $\mathcal{R}$ the weight of toroidal rotation. These relations evidence the tilting of the poloidal asymmetry of the impurity due to parallel friction forces that couple the horizontal and vertical components $(\delta, \; \Delta)$. We obtain with these equations a self-consistent determination of the collisional impurity flux and of the poloidal asymmetry. In contrast with the standard ordering of neoclassical theory, the flux depends here nonlinearly on the impurity gradient through the poloidal asymmetry, as was first investigated by Helander et al [7]. This formulation of the problem can also be expressed in a geometrical way that greatly helps its resolution: poloidal asymmetry parameters describe an ellipsis in the most general case, with a position on the ellipsis (referred to as the collisional angle) that depends on the collisional friction parameter $\mathcal{A}$.

## 1.1 The natural case

In the absence of any toroidal rotation and poloidal asymmetry of the electrostatic potential (what we refer to as the natural case), the poloidal asymmetry parameters of the

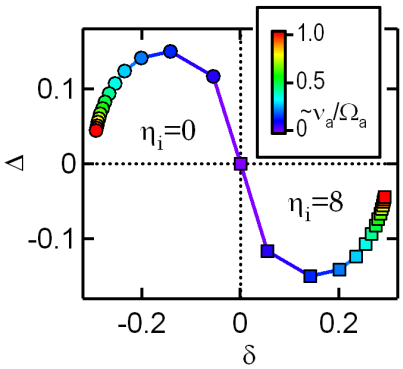



Figure 1: *Poloidal asymmetry for a flat and a peaked temperature profile ($\eta_i = \partial_r \ln T_i / \partial_r \ln N_i$) when increasing the friction $\nu_a$.*

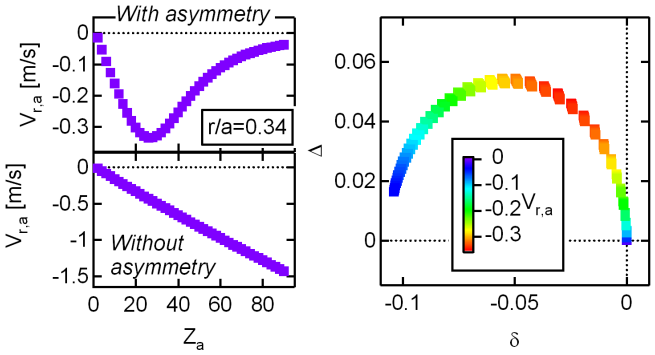



Figure 2: *Radial flow with and without poloidal asymmetry, as a function of the impurity charge, and in the ($\delta$, $\Delta$) plane (right), for a peaked ion density.*

impurity describe a circle crossing the origin. In figure 1, the horizontal ($\delta$) and vertical ($\Delta$) asymmetry parameters are plotted at a given radial position for a flat and a peaked ion temperature profile when increasing the friction with the main ions ($\nu_a/\Omega_a$). The impurity flux is reduced by the growing negative horizontal asymmetry that originates from collisional friction with the main ion when the ion density profile is peaked (fig.2). A similar reduction also arises for a flat ion density case with the formation of a positive horizontal asymmetry. Simulations with XTOR, where the impurity behaviour is described via density and parallel momentum equations, confirm these results via an artificial collisionality scan [4], as shown in figure 3.

It can be shown that in the absence of toroidal rotation or anisotropic electrostatic potential, the steady state impurity distribution is however symmetric, so that the reduction of the flux affects the impurity profile in a transient way (fig. 4,left). Nonlinear simulations also reproduce the theoretical trajectory of the poloidal asymmetry during the evolution to steady state, although the slow dynamics of the impurity profile does not allow following the trajectory up to steady-state (fig. 4,right).

An important extension of the natural case is to allow for a poloidal asymmetry of the electrostatic potential that arises from ion-electron collisions [8] or turbulence [9]. These asymmetries are generally small compared to the ones driven by toroidal rotation or Ion Cyclotron Resonance Heating (ICRH) in the minority scheme, but they can have a very significant effect due to the high electric charge of the impurity. Considering the collisional drive for example, it generates a vertical asymmetry of the electrostatic potential that greatly amplifies the impurity flux. Due to the coupling between the horizontal and vertical asymmetry through collisions, this vertical asymmetry drive also generates a significant horizontal asymmetry that is not captured by the standard neoclassical ordering used for example in NEO. The vertical asymmetry driven by collisions scales as $\nu_i$ : it is

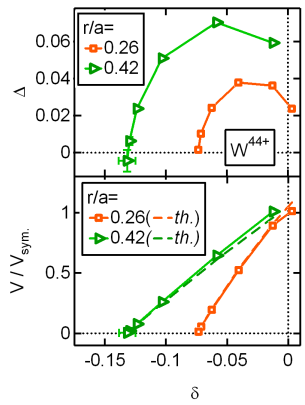



Figure 3: *Poloidal asymmetry variation with the friction on the main ions (top), and pinch velocity reduction by asymmetry in XTOR and in the model ("th.").*

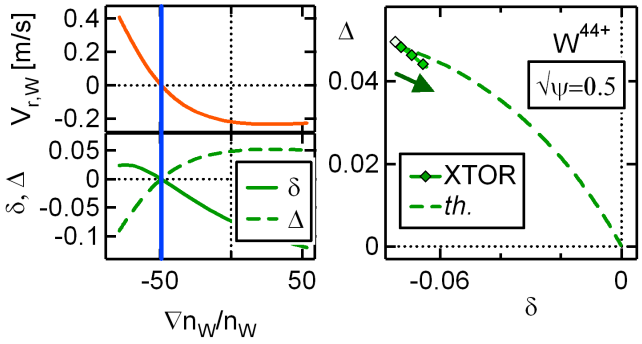



Figure 4: *Left: Radial flow and poloidal asymmetry parameters as a function of impurity gradient. Right: Trajectory towards steady-state in the $(\delta, \Delta)$ plane (right).*

negligible for high temperature plasmas but can be significant in WEST when operating at high density. Regarding the asymmetry drive driven by turbulence, its impact on neoclassical impurity transport must be balanced with the turbulent transport itself, and the overall effect remains to be addressed.

## 1.2 Toroidal rotation and electrostatic potential asymmetry effects

The analytical model covers the effect of toroidal rotation and of electrostatic potential asymmetry, and allows computing experimental situations of interest when using Neutral Beam injection, as well as ICRH when the contribution of the minority thermal screening effect can be neglected. We show in figure 5 the diffusion coefficient, pinch velocity and horizontal asymmetry at $\Gamma^{neo} = 0$ as a function of the ion Mach number for a simple analytical equilibrium, at $r/a = 0.2$. Due to the non linear relation between the gradient and the flux, the zero flux condition must be determined by scanning the impurity gradient, with $D_a$ and $V_a$ being dependent on it. We find that the inward pinch is strongly increased as centrifugal forces push Tungsten to the Low Field Side, in agreement with experimental observations and with computations using NEO. At large Mach number, the pinch velocity is overestimated with the analytical model, due to the simple parametrization of the poloidal asymmetry that becomes inaccurate at these large values.

The ICRH effect is related with the horizontal asymmetry of the electrostatic potential driven by the anisotropic temperature of the minority species:

$$\delta_\phi = \frac{\epsilon}{1 + Z_i T_e / T_i} \left[ f_H \left( \frac{T_\perp}{T_\parallel} - 1 \right) + m_i \frac{(R_0 \Omega)^2}{T_i} \right] \tag{6}$$

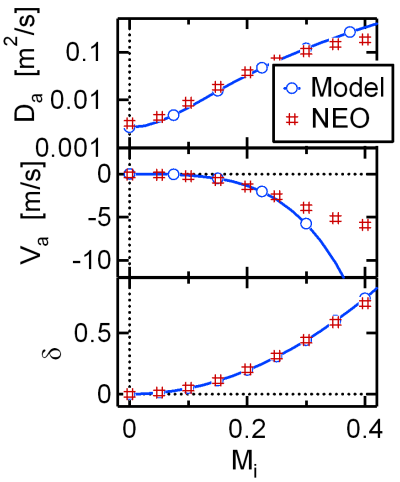



Figure 5: *Neoclassical diffusion coefficient, pinch velocity and horizontal asymmetry as a function of the ion Mach number.*

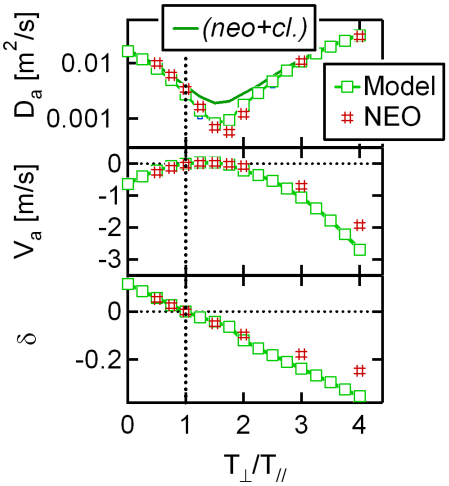



Figure 6: *Neoclassical diffusion coefficient, pinch velocity and horizontal asymmetry as a function of* $T_\perp/T_\parallel$.

By neglecting the minority temperature screening effect, we assume that $f_H R/L_{T,H} \ll R/L_{T,i}$ with $f_H$ the minority fraction. As shown in figure 6, we find that the pinch velocity at $\Gamma^{neo} = 0$ becomes largely inwards as the horizontal asymmetry is becoming negative, except in a narrow window where $T_\perp/T_\parallel$ is just above unity, in agreement with NEO computations. This indicates that, in the absence of toroidal rotation and when neglecting minority thermal screening effect, ICRH has a tendency to drive Tungsten accumulation. This counter intuitive result, with respect to usual experimental observations, could be explained by the fact that the favorable effect of ICRH on Tungsten accumulation is reported in rotating plasmas, where ICRH tends to reduce the strong positive horizontal asymmetry due to centrifugal forces. In fact, when toroidal rotation is considered, the domain of $T_\perp/T_\parallel$ where this particular transition occurs moves towards higher values, and the transition region can be approximated by

$$\left[ f_H \left( \frac{T_\perp}{T_\parallel} - 1 \right) \right]^{crit} \approx 2 \frac{Z_i + T_i/T_e}{Z_a} + 2M_i^2 \left[ \frac{m_a}{m_i} \frac{Z_i + T_i/T_e}{Z_a} - 1 \right] \tag{7}$$

showing that the favorable range where ICRH expels Tungsten from the core expands as the ion Mach number $M_i$ increases. It is worth noting that the neoclassical diffusion becomes extremely small in the transition region between expulsion and accumulation, so that classical transport (also computed in FACIT and shown in the figure) becomes dominant. Even a small level of turbulent transport could significantly reduce the equilibrium Tungsten gradient in this domain of operation: $(\partial_r n_W/n_W)_{eq} = (V^{neo}+V^{cl}+V^{turb})/(D^{neo}+D^{cl}+D^{turb})$.

It is important to note that when reaching an equilibrium situation in a pure neoclassical case (i.e. for $\Gamma^{neo} = 0$), the poloidal asymmetry of the impurity distribution tends to align with that of the drive. It goes formally to zero in the "natural" case, and adopts a nearly pure

horizontal component for rotating plasmas and for cases with a pure horizontal asymmetry of the electrostatic potential, as predicted with models adopting the standard neoclassical ordering assumptions, like the one implemented in NEO. In presence of turbulence, the steady state might however have a remaining tilted asymmetry.

## 2 TUNGSTEN PEAKING DURING ICRH IN WEST

Tungsten accumulation is rarely observed in WEST, and this has been explained by the fact that, due to the low torque exerted by RF heating systems, neoclassical transport was unable to compete with turbulent processes [10, 11]. However, such accumulation is observed in some pulses that therefore deserve particular attention. The FACIT code has been applied to a case with an ICRH power ramp and a temperature collapse occurring above 4 MW of injected power (figure 7). Tungsten accumulation is inferred from the sudden increase of the inverted bolometer signal in the core, leading to a subsequent drop of the core temperature. The mechanisms investigated here are the minority temperature anisotropy, computed with the EVE/AQL code [12], and toroidal rotation, while minority temperature screening is ignored. From EVE/AQL results, this later assumption is only marginally satisfied since we have $f_H \left|\partial_r \ln T_\perp/T_\parallel\right|$ of order unity in the core region. But on the other hand, the temperature anisotropy profile is probably smoother than assumed here, due to finite orbit corrections for example. In any case, we take the results computed here as simple indications of the possible accumulation amplitude that ICRH could generate. Toroidal rotation is not measured on WEST, but this discharge exhibits a $(4, 1)$ MHD mode at around 2.7 kHz that accelerates linearly with the ICRH power up to about 3.7 kHz at $P_{IC} = 4MW$ (figure 9). The $q = 4$ surface is naturally far from the accumulation region, so that we can just assume that toroidal rotation will possibly increase by a similar amount in the core. The magnetic equilibrium is deduced from a METIS interpretative simulation [13] where the ion temperature profile is inferred from the neutron flux with a radial profile proportional to $\sqrt{n_e T_e}$. A general picture of the operational domain is then obtained by scanning the ICRH power and the toroidal rotation for deriving an operational map of the steady state Tungsten peaking factor.

The temperature anisotropy computed with EVE/AQL is shown in figure 10, assuming a minority fraction $f_H = 5\%$. The important factor for neoclassical transport is $f_H(T_\perp/T_\parallel - 1)$, which is taken as proportional to the ICRH power. Concerning toroidal rotation, we assume that the acceleration provided by ICRH is purely toroidal, and from the MHD spectrogram we write it as : $V_\varphi = V_0 + (V/P) \times P_{IC}$ with $V_0 = 0$ or $50$ km/s depending on the ohmic toroidal rotation being either purely poloidal or purely toroidal respectively, $(V/P) \approx 3$ km/s/MW at $q = 4$ and $P_{IC}$ expressed in MW. The results of FACIT computation for this particular case is shown in figure 8, where we display the Tungsten peaking $n_W(0)/n_W(0.3)$ in the $(P_{IC},\ V_\varphi)$ plane, in the limit where turbulent transport is negligible, but taking into account classical transport. The two lines correspond to the two hypotheses on the relation between ICRH power and the induced toroidal rotation.

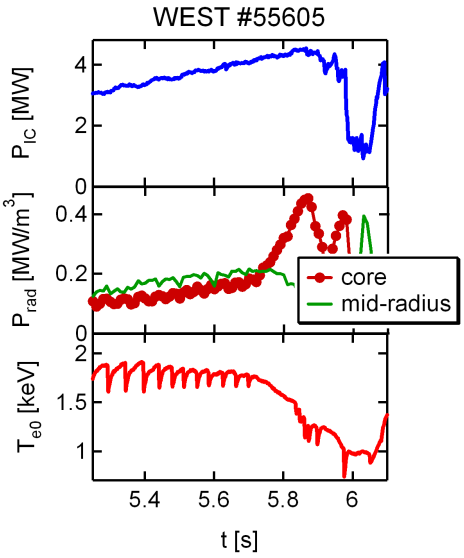



Figure 7: *ICRH power, radiative power and core electron temperature evolution.*

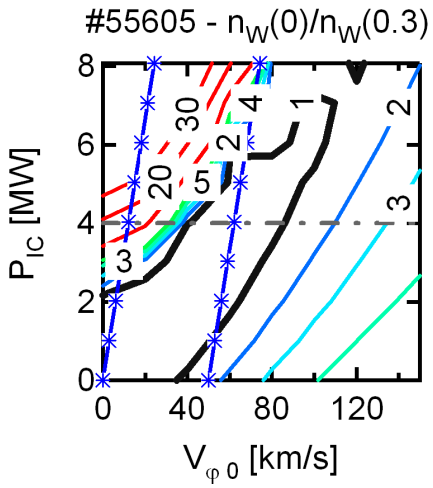



Figure 8: *Steady state Tungsten peaking as a function of toroidal rotation and ICRH power.*

The minimum of Tungsten peaking is observed in the transition region described by eq. (7), where the asymmetry of the electrostatic potential driven by ICRH is compensated by toroidal rotation. On the right of this valley, the accumulation driven by centrifugal forces dominates, while on the left, Tungsten accumulation is driven by ICRH. Following this diagram, the observed accumulation at $P_{IC} = 4$MW is consistent with a moderate toroidal rotation, and an accumulation driven by ICRH.

## 3 SUMMARY

A fast analytical method, implemented in the FACIT code, allows computing the collisional impurity transport in the Pfirsh-Schlüter regime, including toroidal rotation and electrostatic potential asymmetry effects. It makes no assumption on the ordering of collisional friction in the parallel force balance, and thus includes self-consistently a tilting of the impurity poloidal distribution with respect to the asymmetry drives. This tilting can have a strong impact in regimes where these drives are small (the so-called "natural" case). As a consequence also, the impurity flux is a non-linear function of the impurity gradient. The analytical model has been applied to a rare WEST case where Tungsten accumulation is observed with ICRH. The steady state Tungsten peaking computed with FACIT is shown to be strongly increased with ICRH power at low rotation, a situation that could be relevant for the experiment considered. Minority temperature screening effect, not considered in this preliminary study, could bring new elements for explaining these observations.

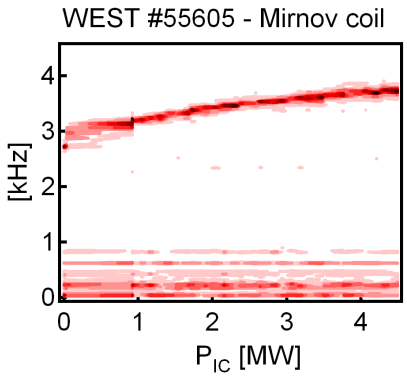



Figure 9: *MHD spectrogram as a function of ICRH power.*

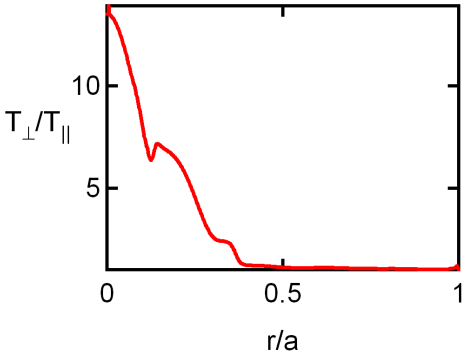



Figure 10: *Minority temperature anisotropy profile computed with EVE/AQL ($f_H = 5\%$).*

# Acknowledgments

This work has been carried out within the framework of the EUROfusion Consortium and the French Research Federation for Fusion Studies and has received funding from the Euratom research and training programme 2014-2018 and 2019-2020 under grant agreement No 633053 for the project ENR-MFE19.CEA-03. We benefited from HPC resources from GENCI (project 056348). The views and opinions expressed herein do not necessarily reflect those of the European Commission.

# References

[1] MAGET P. ET AL. *Plasma Physics and Controlled Fusion* **62** (2020) 105001.
[2] LÜTJENS H. ET AL. *Plasma Physics and Controlled Fusion* **51** (2009) 124038.
[3] AHN J.H. ET AL. *Plasma Physics and Controlled Fusion* **58** (2016) 125009.
[4] MAGET P. ET AL. *Plasma Physics and Controlled Fusion* **62** (2020) 025001.
[5] BELLI E.A. ET AL. *Plasma Physics and Controlled Fusion* **50** (2008) 095010.
[6] ANGIONI C. ET AL. *Plasma Physics and Controlled Fusion* **56** (2014) 124001.
[7] HELANDER P. *Physics of Plasmas* **5** (1998) 3999.
[8] HINTON F.L. ET AL. *The Physics of Fluids* **16** (1973) 836.
[9] ESTÈVE D. ET AL. *Nuclear Fusion* **58** (2018) 036013. DONNEL P. ET AL. *Plasma Physics and Controlled Fusion* **61** (2018) 014003. DONNEL P. ET AL. *Plasma Physics and Controlled Fusion* **61** (2019) 044006.
[10] YANG X. ET AL. *Nuclear Fusion* **60** (2020) 086012.
[11] GONICHE M. ET AL. *this conference*. BUCALOSSI J. ET AL. *this conference*.
[12] DUMONT R. *Nuclear Fusion* **49** (2009) 075033. DUMONT R. ET AL. *Nuclear Fusion* **53** (2012) 013002.
[13] ARTAUD J. ET AL. *Nuclear Fusion* **58** (2018) 105001.